Full-waveform Based Complete Moment Tensor Inversion and Stress Estimation from Downhole Microseismic Data for Hydrofracture Monitoring

Fuxian Song[1], M. Nafi Toksöz[1]

[1] *Earth Resources Laboratory, Massachusetts Institute of Technology, Building 54-614, 77 Massachusetts Ave, Cambridge, MA 02139, USA, E-mail: fxsong@mit.edu*

Abstract

Downhole microseismics has gained increasing popularity in recent years as a way to characterize hydraulic fracturing and to estimate in-situ stress state. Conventional approaches only utilize part of the information contained in the microseismic waveforms such as the P/S far-field amplitudes to determine the focal mechanisms and infer stress state. The situation becomes more serious for downhole monitoring where only limited azimuthal coverage is available. In this study, we developed a full-waveform based approach to invert for complete moment tensor. We use the discrete wavenumber integration method as the fast forward modeling tool to calculate the full wavefield in the layered medium. By matching the waveforms across the array, a stable moment tensor solution can be obtained without imposing additional constraints. We show that by using full waveforms, the resolution of the full seismic moment tensor is improved even with data from a single monitoring well. We also determine the stress drop from the S-wave

displacement spectrum. We test our method using a downhole microseismic dataset from hydraulic fracturing treatments in East Texas. The results indicate the existence of non-double-couple components in the moment tensor. The derived fracture plane direction also agrees with that derived from multiple event location.

Introduction

Microseismic downhole monitoring is a valuable tool for fracture mapping. The locations of microseismic events, with sufficient resolution, provide information on fracture geometry and properties (Warpinski et al., 1998; Phillips et al., 2002). Besides location, seismic moment tensor is also derived to understand the microseismic source mechanisms and stress state (Nolen-Hoeksema and Ruff, 2001; Baig and Urbancic, 2010). Currently, most moment tensor inversion methods rely only on far-field P- and S-wave amplitudes. Thus, they normally either require multiple wells at different azimuths or make additional double-couple source assumption when data from only one monitoring well is available, as is the typical case for hydraulic fracturing (Vavrycuk, 2007; Baig and Urbancic, 2010).

In this paper, we propose a full-waveform approach for moment tensor inversion using data from one monitoring well. It uses the discrete wavenumber integration method to calculate elastic wave-fields in the layered medium. By matching full waveforms across the geophone array, we show that the inversion can be stabilized so that the complete moment tensor can be retrieved from data recorded in a single borehole. In this paper, we begin by introducing the full-waveform approach and testing the method with synthetic data. Then we describe the application to a field dataset from East Texas. We

invert the complete seismic moment tensor and extract three characteristic parameters: seismic moment, fracture orientation, and the isotropic component percentage. The stress drop is also derived from the S-wave displacement spectrum based on Madariaga's model (Madariaga, 1976).

Methodology

Full waveform based complete moment tensor inversion

The moment tensor of microseismic events can be represented by a 3 by 3 symmetric matrix (Aki and Richards, 2002). The complete moment tensor is defined as the 6 independent components of the moment tensor matrix. To improve the inversion with a single borehole coverage, we use all phases that are embedded in the full waveform data. Our approach starts from full elastic waveform modeling in the layered medium with discrete wavenumber integration method (DWN; Bouchon, 2003). The i-th component (North, East, Down) of the observed waveform at geophone n is modeled as:

$$v_i(x_r^n, x_s, t) = \sum_{j=1}^{3}\sum_{k=1}^{3} m_{jk}\, G_{ij,k}(x_r^n, x_s, t) * s(t)\,, \tag{1}$$

where $*$ denotes convolution (same hereinafter); $G_{ij,k}(x_r^n, x_s, t)$ is the i-th component of the Green's function at geophone x_r^n from a point moment tensor source m_{jk} at x_s; $s(t)$ is the source time function. In this study, a smooth ramp function is used as $s(t)$.

The misfit function for inverting moment tensor matrix m_{jk} is defined by:

$$\Delta(m_{jk}) = \sum_{n=1}^{N}\sum_{i=1}^{3}\int_0^{T_n}\left(d_i(x_r^n, x_s, t) - v_i(x_r^n, x_s, t)\right)^2 dt\,, \tag{2}$$

where $d_i(x_r^n, x_s, t)$ is the observed data, while $v_i(x_r^n, x_s, t)$ is the synthetic data as described in equation 1. T_n is the duration of observed waveforms at geophone n. In this

study we choose T_n to include both P and S wave trains and keep it constant for all geophones. Time 0 is the origin time, which is obtained by a grid-search around its initial estimate within the dominant signal period. The initial estimate of the origin time can be found by cross-correlating the synthetic and observed waveforms. To further stabilize the inversion, both synthetic data and observed data are band-pass filtered. Based on the spectral analysis of field data, a signal frequency band of [200, 900] Hz is used in this study. The moment tensor is solved by minimizing the misfit function in equation 2 as:

$$M_i(x_s) = (A^{-1})_{ij}(x_s) D_j(x_s)\ , \tag{3}$$

Here M_i is the i-th component of six independent moment tensor elements: $M_1 = m_{11}$, $M_2 = m_{22}$, $M_3 = m_{33}$, $M_4 = m_{12}$, $M_5 = m_{13}$, $M_6 = m_{23}$, while D_j has six independent elements, representing the correlation between observed data and synthetic seismograms resulting from the six independent moment tensor elements:

$$D_j(x_s) = \sum_{n=1}^{N} \sum_{k=1}^{3} \int_0^{T_n} g_{kj}(x_r^n, x_s, t) d_k(x_r^n, x_s, t) dt\ , j = 1,2,3 \ldots 6. \tag{4}$$

g_{kj} corresponds to one of the six seismograms defined by:

$$g_{kj}(x_r^n, x_s, t) = G_{kj,j}(x_r^n, x_s, t) * s(t)\ ,\ j = 1,2,3, \tag{5}$$

$$g_{k4}(x_r^n, x_s, t) = \left[G_{k2,1}(x_r^n, x_s, t) + G_{k1,2}(x_r^n, x_s, t)\right] * s(t)\ , \tag{6}$$

$$g_{k5}(x_r^n, x_s, t) = \left[G_{k3,1}(x_r^n, x_s, t) + G_{k1,3}(x_r^n, x_s, t)\right] * s(t)\ , \tag{7}$$

$$g_{k6}(x_r^n, x_s, t) = \left[G_{k2,3}(x_r^n, x_s, t) + G_{k3,2}(x_r^n, x_s, t)\right] * s(t)\ . \tag{8}$$

Finally, matrix A is a 6*6 matrix with elements:

$$A_{ij}(x_s) = \sum_{n=1}^{N} \sum_{k=1}^{3} \int_0^{T_n} g_{kj}(x_r^n, x_s, t) g_{ki}(x_r^n, x_s, t) dt\ . \tag{9}$$

The seismic moment is derived from the moment tensor matrix m_{jk} as:

$$M_0 = max|\lambda_i|\,, \tag{10}$$

where λ_i is the eigenvalue of the moment tensor matrix. The moment magnitude is defined as:

$$M_w = \frac{2}{3} log_{10}(M_0) - 6.607\,, \tag{11}$$

where M_0 is the seismic moment in N*m.

The full moment tensor matrix is further decomposed into three parts: isotropic (ISO) component, compensated linear vector dipole (CLVD) component and double-couple (DC) component (Vavrycuk, 2001). The fracture strike is then derived from the DC component (Jost and Hermann, 1989). The ISO component percentage is determined by:

$$c^{ISO} = \frac{1}{3}\frac{\text{trace}(m_{jk})}{M_0}100\%\,. \tag{12}$$

Stress drop estimation

According to (Madariaga, 1976), the radius of a circular source is estimated as:

$$r_0 = \frac{1.32\bar{V}_s}{2\pi f_c}, \tag{13}$$

where f_c is the corner frequency derived from S-wave displacement spectrum and $\bar{V}_s$ is the average S-wave velocity of the medium. Stress drop, defined as the average difference between the initial and final stress levels over the fault plane, is obtained from:

$$\Delta\sigma = \frac{7}{16}\frac{M_0}{r_0^3}, \tag{14}$$

where M_0 is the seismic moment determined by complete moment tensor inversion as shown in equation 10.

Synthetic study

Full waveform fitting and complete seismic moment tensor inversion

In this section, we study the influence of borehole azimuthal coverage on complete moment tensor inversion and compare the full-waveform approach with conventional methods using far-field P/S amplitudes. Next, we show an example of full waveform source inversion for a double-couple source with additive Gaussian noise. We demonstrate the waveform fitting results and compare the inverted source parameters to the exact values.

The 1D velocity model derived from the field experiment, as shown in Figure 1, is used throughout this paper to generate synthetics and perform inversion. We assume a known velocity model and source location. The justification for these assumptions is explained in the field study section. Firstly, we study the influence of borehole azimuthal coverage on the full waveform based complete moment tensor inversion. We limited our analysis to the noise free case to investigate the effect of well coverage. The influence of noise is discussed afterwards.

As shown in Figure 2 (a), a tensile earthquake model is used to describe the microseismic source. The fault is vertical in the N-S direction (strike value = 0^0). The slip lies in the horizontal plane and slip azimuth α changes from 0^0 to 180^0. The microseismic source, labeled as plus sign in Figure 2 (b), lies in the center of the circle, with 8 monitoring wells, B1 to B8, spreading from the North direction to the North-West direction. The azimuthal difference between two adjacent wells is 45^0. To mimic the field setup, the source is located at a depth of 3975 m (13042 ft) and 101 m (331 ft) away from

the monitoring wells. In each well, a six-geophone array is deployed at a depth from 3912 m (12835 ft) to 3944 m (12940 ft). Figure 3 gives the calculated percentages of the ISO, DC and CLVD components for the tensile earthquake model of Figure 2(a) using equation (8) of Vavrycuk (2001). If the slip azimuth α equals to 0^0 or 180^0, the source is pure shear with no ISO or CLVD components. When the slip azimuth changes to 90^0, a pure tensile source is generated. The double-couple percentage is zero, and the ISO and CLVD components are positive and attain their maximum values. For the other slip directions, the source is mixed. All three components exist.

Four sets of synthetic experiments are conducted: 1) full azimuthal coverage, using all eight boreholes, B1 to B8; 2) partial azimuthal coverage, using the two boreholes, B1 and B2; 3) a single well coverage using the borehole B1 at an azimuth of 0^0 east of north; 4) a single well coverage using the borehole B2 at an azimuth of 45^0 east of north. For each set of experiment, the full waveform based complete moment tensor inversion is conducted on the synthetic data using the exact velocity model and the accurate source location. Four characteristic source parameters including strike, seismic moment, ISO and DC component percentage are then estimated from inverted moment tensors and compared with the exact values. The errors are calculated as the difference between the exact values and the estimated values.

The errors in the inverted source parameters, as a function of the slip direction, are plotted in Figure 4 for four cases: (a) eight boreholes, (b) two boreholes at an azimuth of 0^0 and 45^0, (c) one borehole at an azimuth of 0^0, and (d) one borehole at an azimuth of 45^0. Figure 4 indicates that for all slip azimuths, the source parameters can be correctly retrieved by the full-waveform based approach even with a single vertical borehole,

which is impossible for conventional approaches based only on far field P/S amplitudes (Vavrycuk, 2007; Eaton, 2009). A further study suggests that the improvement brought by the full-waveform based method is also seen as a decrease in the condition number of the matrix A. The improvement may come from two sources: 1) more angular coverage of the source is achieved by using full waveforms in the layered medium instead of a homogeneous medium, and 2) near field wave-field helps retrieve the moment tensor components not recoverable from conventional moment tensor inversion methods.

Two more observations are made from Figure 4. Firstly, in all cases, the smallest error in the inverted source parameters is achieved for pure DC sources, that is, for the slip azimuths of 0^0 and 180^0. For pure DC sources, the full-waveform approach loses most of its benefits, since the conventional method, which uses far field P/S amplitudes and makes additional double-couple source assumption, can also retrieve correct complete moment tensor (Vavrycuk, 2007). Secondly, the errors in the strike estimate for a pure tensile source (i.e., the slip azimuth of 90^0) reaches its maximum of around -4^0 when only one borehole at an azimuth of 45^0 away from the strike direction (N-S direction) is available, while the error reduces to -0.4^0 when one monitoring well is located in the strike direction (i.e., at an azimuth of 0^0). This suggests that when only one monitoring well is allowed, it is better to place it close to the strike direction if a-priory information on major fault orientation is available.

Next, we demonstrate the full-waveform approach on a noisy synthetic dataset. In this experiment, a double-couple source (strike: 85^0 degrees, dip: 75^0, rake: 0^0), located at a depth of 3975 m (13042 ft) and 65 m (213 ft) north, 77 m (254 ft) west away from a six-geophone downhole array, is assumed. The geophone array is kept at the same location as

the previous noise-free experiment. Knowing the layered velocity model, as depicted in Figure 1, the source, and the geophone array, DWN is used to generate the noise-free data. Next, a 10% Gaussian noise is added to form the synthetics for moment tensor inversion. All three-component data are included in the inversion.

As an example, Figure 5 gives the vertical component fitting between synthetic data (in red) and inverted data (in blue). A good agreement is observed for both P- and S-waves. Moreover, a reasonable fit for the converted wave is also seen. Good agreements are also seen on East and North component data. Compared to conventional methods using only far-field P and S first-arrival amplitudes, it is found that, the condition number of the matrix A is reduced by at least one order of magnitude using data from a single vertical well. This explains why we can invert for complete moment tensor from a single borehole by using full waveforms. The inverted moment tensor gives a fracture plane with strike of 84.9 degrees, dip of 74.5 degrees, and rake of -0.6 degrees, which is close to the true orientation.

Seismic moment estimate

To evaluate the accuracy of the seismic moment estimated by our method, we conduct a Monte Carlo simulation. In this experiment, we fix the source location at (N, E, D) = (64.8, 77.3, 3975.3) m and a source mechanism of (strike, dip, rake) = (85^0, 75^0, 0^0). We vary the seismic moment from 10^3 N·m to 10^8 N·m. For different seismic moment values, different realizations of 10% Gaussian noise are added to the synthetic data to study the statistical properties of the seismic moment estimator. For each seismic moment value, a full-waveform moment tensor inversion as described above is performed to retrieve the seismic moment.

Figure 6 gives the comparison between the true seismic moment used to generate synthetics and the estimated seismic moment by full moment tensor inversion. The estimated seismic moment values agree well with the true seismic moment values. The mean error is around 3.9%, while the standard deviation is about 5.2%. This means that true values of M_0 are within the confidence region of the estimated M_0 under additive Gaussian noise, which is consistent with previous study (Patton and Aki; 1979). The non-zero bias comes from two parts: 1) the errors propagated into the moment tensor inversion solution due to the additive data noise, which is well bounded by the illness of matrix A; 2) the numerical errors from the eigenvalue decomposition as described in equation 10. In summary, for a broad range of seismic moment values, our method gives a good estimate.

Strike estimate

A similar Monte Carlo simulation has been conducted to assess the performance of strike estimator. For this test, we test two source mechanisms. One is the pure double-couple mechanism, while the other is a mixed source with a 60% double-couple component and a 40% isotropic component. For both scenarios, the dip and rake value is set to be 75^0 and 0^0, respectively. We also fix the source location same as in previous section and use a constant seismic moment of $5*10^4$ N·m. The strike value is changed from 0^0 to 360^0. For each strike value, a forward modeling with 10% additive Gaussian noise is conducted and a full-waveform moment tensor inversion is performed afterwards to invert for the full moment tensor and retrieve the strike.

The estimated strike is plotted against the true strike for both cases in Figures 7 (a) and (b). The estimated strike is in good agreement with the true value. The strike estimate has

a mean error of -0.1 degrees from the true value for the pure DC source, while the mean error increases to 0.3 degrees for the isotropic plus double-couple source. The increased error in strike for the mixed source case is probably due to the decreased deviatoric part of the seismic moment tensor, from which the strike is defined.

Isotropic component percentage estimate

The isotropic component percentage defined in equation 12 provides a good indicator of fracture volumetric strain. It gives some idea about fracture opening and closure. As discussed in previous section on strike estimate, it also indicates the uncertainty of strike estimates to some degree. The higher the isotropic component percentage is, the less accurate the strike estimate can be.

In this experiment, we change the relative percentage between the DC component and ISO component and fix the seismic moment to be $5*10^4$ N·m. All other parameters are kept the same as the section on seismic moment estimate. Figure 8 represents the comparison between the true isotropic percentage and estimated isotropic percentage. The estimated ISO percentage generally agrees well with the true ISO percentage. There is some scattering for the estimates due to 10% Gaussian noise. The mean error is around -0.2%, while the standard deviation approaches 2.6%. This means the true ISO percentage value falls into the confidence region of the estimated isotropic percentage, although the maximum absolute error is close to 8%.

Field study

Field setup

A microseismic survey was conducted during the hydraulic fracturing treatment of the Bonner sands in the Bossier play at a depth approximately from 3956 m (12980 ft) to

3981 m (13060 ft). The microseismic data was collected using a twelve-level, three-component geophone array deployed in the vertical monitoring well at a depth from 3874 m (12710 ft) to 3944 m (12940 ft). The treatment well is approximately 151 m (495 ft) away from the monitoring well. The recorded data was analyzed and located for hydraulic fracturing mapping as outlined by Griffin et al. (2003), and Sharma et al. (2004). The velocity model for location, shown in Figure 1, was derived from the well logging data and calibrated using perforation shots (Warpinski et al., 2003). It also accommodated the local geology information. Thus, it is reasonable to assume the velocity model and location are accurate for source inversion.

In this study, we test our method on several located microseismic events to invert for the complete moment tensor and estimate the stress drop from the full waveforms. The microseismic data from the lower six geophones at a depth from 3912 m (12835 ft) to 3944 m (12940 ft) are selected due to their higher signal-to-noise ratios (SNRs). Figure 9 shows the horizontal plane view of the monitoring well at the origin and seven selected test events in green. A major fracture plane along the N87^{0}E direction is clearly seen (Sharma et al., 2004).

In the following section, we will begin with one event, named test event 1, to demonstrate the procedure for full-waveform based moment tensor inversion and stress drop estimation. After that, we will present and discuss the results for all seven chosen events.

Moment tensor inversion and stress drop estimation

As described in the methodology section, the complete moment tensor is firstly inverted from the full waveforms. Next, three characteristic parameters are extracted: 1)

seismic moment, 2) strike, and 3) the isotropic component percentage. Figures 10 a) and b) give the waveform fitting for test event 1 between synthetics and observed data. Only horizontal components are used because of the poor SNR associated with poor receiver coupling in the vertical component. A good agreement of dominant P and S wave trains is seen in both Figures 10 a) and b). The un-modeled wave packages are probably due to the scattering from the un-modeled lateral heterogeneity.

The estimated seismic moment, strike and the isotropic percentage for event 1 are listed in Table 1. A negative isotropic component indicates some degree of fracture closure. The seismic moment for event 1 is around $6.1*10^4$ N·m, suggesting a moment magnitude around -2.87. The two strike values estimated from the deviatoric component correspond to the orientation of the fracture plane and the auxiliary plane respectively. It is hard to distinguish the two planes using only one event. The estimated strike values for all seven events are listed in Table 1. The first set of strike values agrees well with the strike of $N87^0E$ derived from multiple event location by Sharma et al. (2004), and gives the fracture plane strike. The scattering around $N87^0E$ is due to the fact that the orientation of small local fractures given by individual microseismic events differs from the average fracture orientation represented by multiple event location. Moreover, noise contamination may also contribute to the scattering through the propagation into the inverted moment tensor.

To estimate the stress drop, Madariaga's model is adopted to estimate the source radius from the S-wave corner frequency (Madariaga, 1976). The recorded voltage data is firstly converted to displacement considering the geophone response (Warpinski, 2009). The spectral analysis is then applied to the converted S-wave displacement data. For test event

1, Figure 11 shows the S-wave displacement spectrum and the best-fit curve determined from the kinematic model defined by the following equation:

$$U(f) = \frac{\Omega_0 e^{-\pi f R/\bar{V}_S Q_S}}{1+(f/f_c)^2}, \tag{15}$$

where $\boldsymbol{R}$ is the is the source-receiver distance, Qs = 100 is the S-wave quality factor. In the present case of event 1, average values of 2605 m/s and 112 m are accepted for the S-wave velocity and the source-receiver distance separately. A simple nonlinear-least square inversion is deployed to estimate corner frequency $\boldsymbol{f_c}$ (Talebi and Boone, 1998). Source radius $\boldsymbol{r_0}$ is then derived from $\boldsymbol{f_c}$ according to equation 13. The stress drop is finally determined from previously obtained source radius and seismic moment by equation 14. The stress drop values for all seven events are listed in Table 1. It is seen from Table 1 that the moment magnitudes of all events fall into the range between -4 and -2, which is consistent with previous studies on moment magnitude of hydrofrac events from downhole observations (Warpinski, 2009).

Conclusions

In this paper, we developed a full-waveform based moment tensor inversion approach for hydraulic fracture monitoring using downhole microseismic data. By exploring full waveform information in a layered medium instead of using only P/S far-field amplitudes, we have demonstrated that the complete moment tensor inversion can be stabilized even with one single borehole. By synthetic test, we have shown that the fracture geometry can be reliably derived from the full waveform analysis approach assuming a known velocity model and source location. Synthetic tests also show that additive Gaussian noise does not pose difficulties for recovering reliable estimates of the moment tensor. Moment

tensor inversion of field data indicates the existence of both double-couple and non-double-couple components in the source. The strike values, derived by the inversion, for all test events agree well with the fracture azimuth determined from multiple event location.

Potential errors in source parameter estimates primarily come from the inaccuracies in source locations and velocity models. Future work includes investigating possible effects of errors in source locations and velocity models. This full-waveform approach has the potential to improve the source properties study of microseismic events monitored using borehole sensors even in a single well.

Acknowledgements

The authors would like to thank Pinnacle - A Halliburton Service for providing the data and for funding this research. We are grateful to Dr. Norm Warpinski, Dr. Jing Du, Dr. Erkan Ay and Dr. Qinggang Ma from Halliburton Energy Services Company; Dr. H. Sadi Kuleli and Dr. Michael Fehler from MIT for their helpful suggestions. We thank Halliburton Energy Services Company and Anadarko Petroleum Corporation for permission to publish this work.

References

Aki, K., and P. G. Richards, 2002, Quantitative seismology, 2nd ed.: University Science Books.

Baig, A., and T. Urbancic, 2010, Microseismic moment tensors: A path to understanding frac growth: The Leading Edge, **29**, 320-324.

Bouchon, M., 2003, A review of the discrete wavenumber method: Pure and Applied Geophysics, **160**, 445-465.

Eaton, D. W., 2009, Resolution of microseismic moment tensors: A synthetic modeling study: 79th Annual International Meeting, SEG, Expanded Abstracts, 3569-3573.

Griffin, L.G., R.B. Sullivan, S.L. Wolhart, C.K. Waltman, C.A. Wright, L. Weijers, and N.R. Warpinski, 2003, Hydraulic Fracture Mapping of the High-Temperature, High-Pressure Bossier Sands in East Texas: SPE Annual Technical Conference and Exhibition, Denver, 5-8 October 2003, Paper 84489.

Jost, M.L., and R.B. Herrmann, 1989, A student's guide to and review of moment tensors: Seismological Research Letters, **60**, 37-57.

Madariaga, R., 1976, Dynamics of an Expanding Circular Fault: Bulletin of the Seismological Society of America, **66**, 639–666.

Nolen-Hoeksema, R.C., and L.J. Ruff, 2001, Moment tensor inversion of microseisms from the B-sand propped hydrofracture, M-site, Colorado:Tectonophysics, **336**, 163-181.

Patton, H., and K. Aki, 1979, Bias in the estimate of seismic moment tensor by the linear inversion method: Geophysical Journal International, **59**, 479-495.

Phillips, W., J. Rutledge, and L. House, 2002, Induced microearthquake patterns in hydrocarbon and geothermal reservoirs: six case studies: Pure and Applied Geophysics, **159**, 345-369.

Sharma, M.M., P.B. Gadde, R. Sullivan, R. Sigal, R. Fielder, D. Copeland, L. Griffin, and L. Weijers, 2004, Slick Water and Hybrid Fracs in the Bossier: Some Lessons Learnt:

SPE Annual Technical Conference and Exhibition, Houston, 26–29 September 2004, Paper 89876.

Talebi, S., and T.J. Boone, 1998, Source parameters of injection-induced microseismicity: Pure and Applied Geophysics, **153**, 113-130.

Vavrycuk, V., 2001, Inversion for parameters of tensile earthquakes: Journal of Geophysical Research, **106(B8)**, 16339-16355.

Vavrycuk, V., 2007, On the retrieval of moment tensors from borehole data: Geophysical Prospecting, **55**, 381-391.

Warpinski, N.R, 2009, Microseismic monitoring: inside and out: Journal of Petroleum Technology, **61**, 80-85.

Warpinski, N.R., P.T. Branagan, S.L. Wolhart, and J.E. Uhl, 1998, Mapping hydraulic fracture growth and geometry using microseismic events detected by a wireline retrievable accelerometer array: SPE Gas Tech. Symp., Calgary, 15-18 March 1998, Paper 40014.

Warpinski N.R., R.B. Sullivan, J.E. Uhl, C.K. Waltman, and S.R. Machovo, 2003, Improved microseismic fracture mapping using perforation timing measurements for velocity calibration: SPE Paper 84488.

List of Figures

Figure 5. Synthetic example: vertical component fitting with 10% Gaussian noise added to synthetic seismograms shown in red. The fitted data derived from moment tensor inversion is plotted in blue.

Figure 6. Comparison of the true and estimated seismic moment based on a Monte Carlo simulation with 10% additive Gaussian noise.

Figure 7. Comparison of the true and estimated strike based on a Monte Carlo simulation with 10% additive Gaussian noise, (a) a pure DC source, and (b) a mixed source (60% DC component + 40% ISO component).

Figure 8. Comparison of the true and estimated isotropic percentage based on a Monte Carlo simulation with 10% additive Gaussian noise.

Figure 9. Horizontal plane view of microseismic event locations. Seven selected test events are shown in green.

Figure 10. Comparison between the synthetics and observed data for test event 1: a) North component, b) East component.

Figure 11. S-wave displacement spectrum of test event 1. The observed spectrum is shown in blue, and the model fitted result is plotted in red.

List of Tables

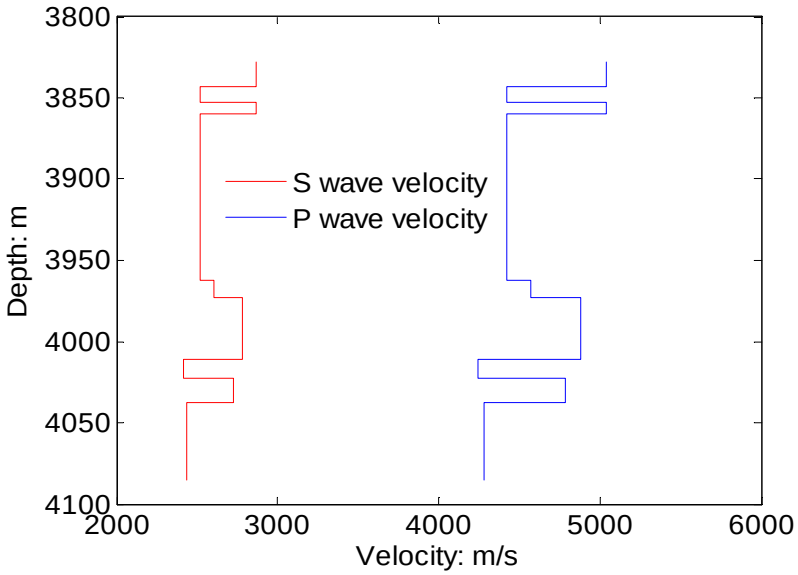

Figure 1. One-dimensional P- and S-wave velocity model derived from field study.

a)

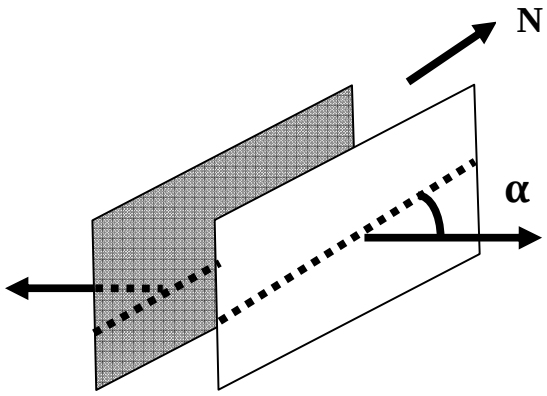

b)

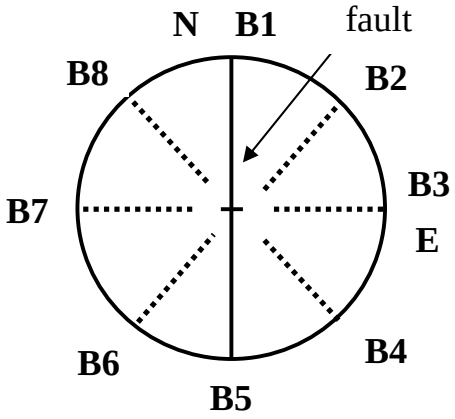

Figure 2. (a) A model for tensile earthquake. The fault is vertical in the N-S direction (strike value = 0). The slip lies in the horizontal plane. Slip azimuth α changes from 0 to 180 degrees. (b) The configuration of numerical experiment in the upper-hemisphere equal-area projection. The microseismic source, labeled as plus sign, lies in the center of the circle, with 8 monitoring wells, B1 to B8, spreading from the North direction to the North-West direction. The azimuthal difference between two adjacent wells is 45^0.

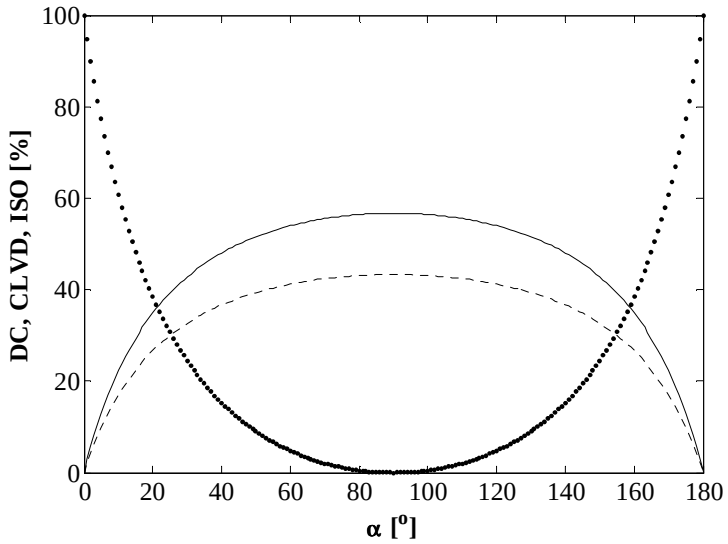

Figure 3. The double-couple and non-double-couple components of the moment tensor for the tensile earthquake model, described in Figure 2. The percentages of DC (dotted line), CLVD (dashed line), and ISO (isotropic) (solid line) components are shown as a function of the slip azimuth α.

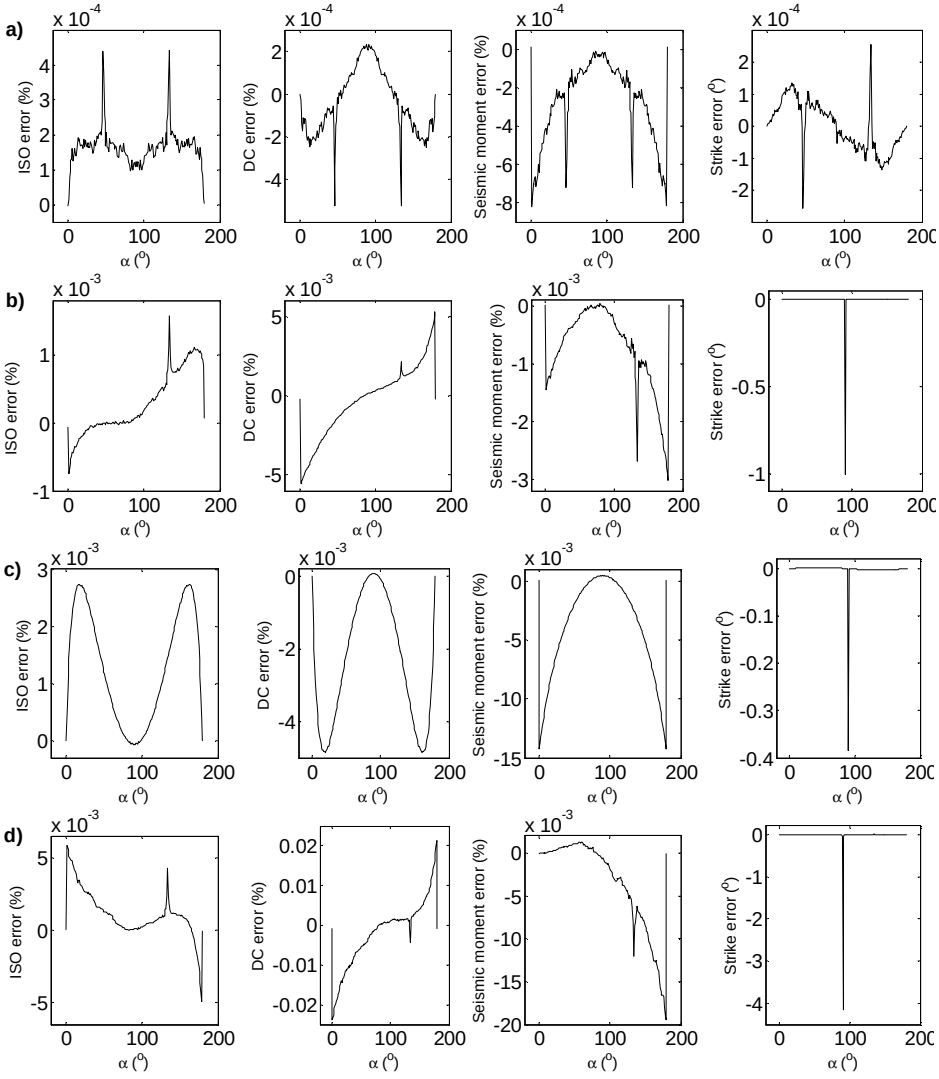

Figure 4. The errors in the inverted source parameters, ISO percentage, DC percentage, seismic moment and strike, as a function of the slip azimuth α under different azimuthal coverage: (a) eight boreholes, (b) two boreholes at an azimuth of 0 and 45 degrees, (c) one borehole at an azimuth of 0 degree, (d) one borehole at an azimuth of 45 degrees. The errors are calculated as the difference between the exact values and the calculated values derived from the inverted complete moment tensor. The inversion is performed using the exact velocity model and the accurate source location.

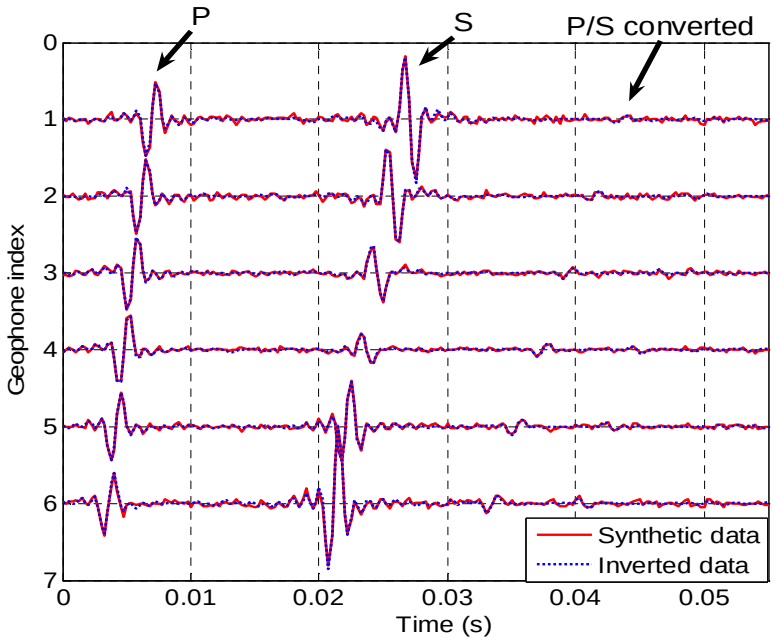

Figure 5. Synthetic example: vertical component fitting with 10% Gaussian noise added to synthetic seismograms shown in red. The fitted data derived from moment tensor inversion is plotted in blue.

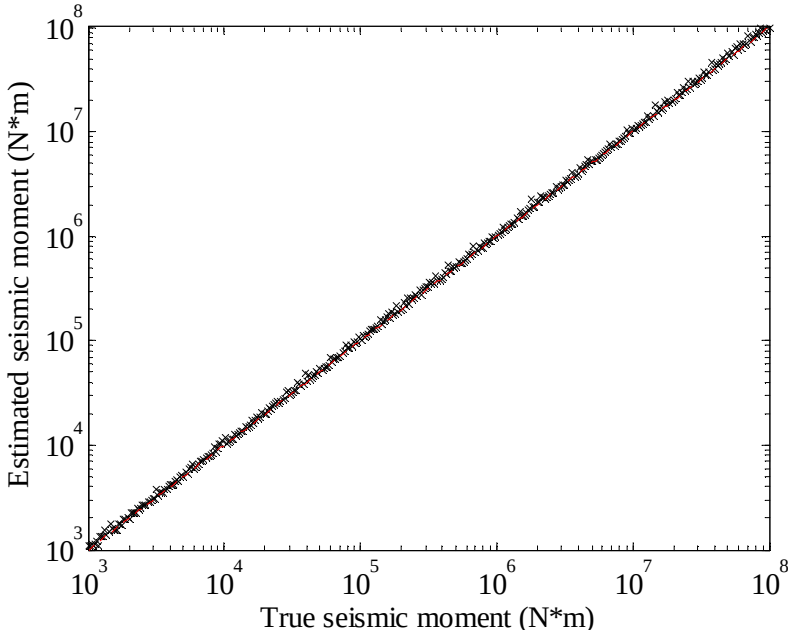

Figure 6. Comparison of the true and estimated seismic moment based on a Monte Carlo simulation with 10% additive Gaussian noise.

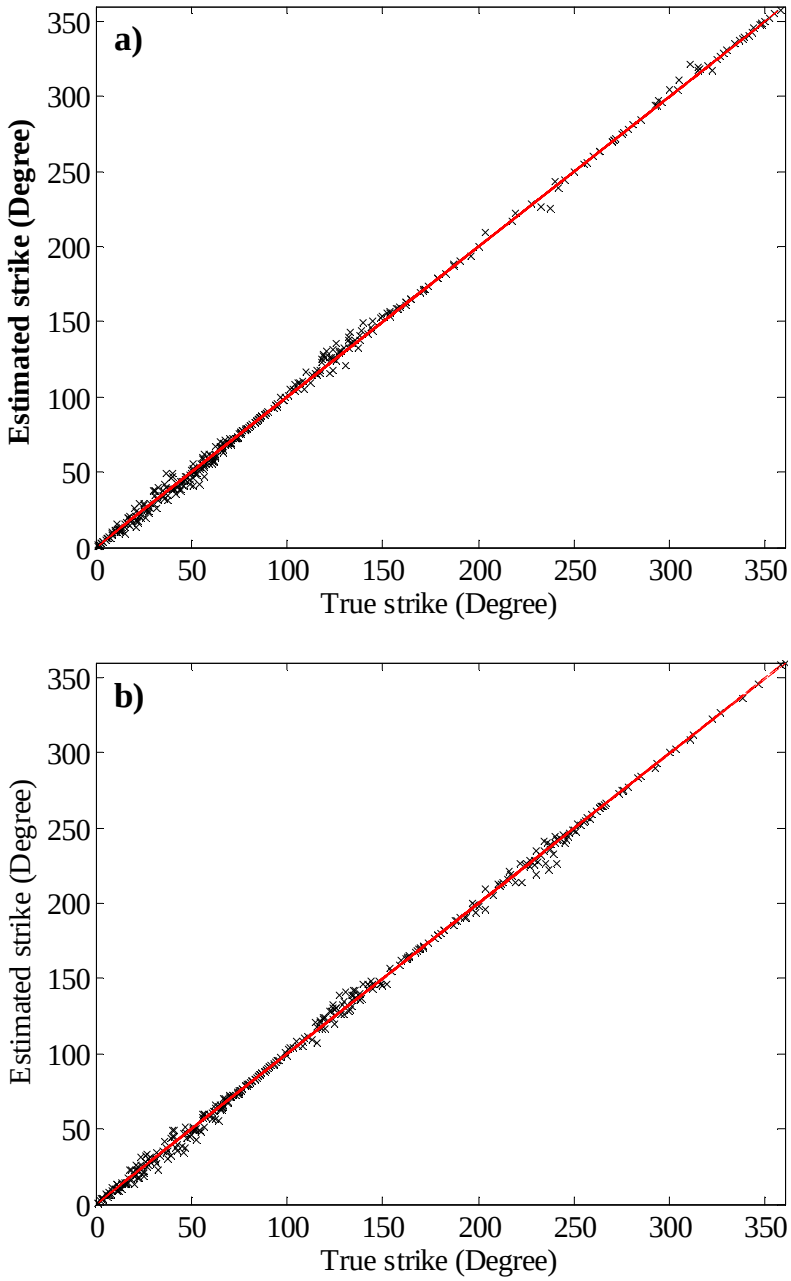

Figure 7. Comparison of the true and estimated strike based on a Monte Carlo simulation with 10% additive Gaussian noise, (a) a pure DC source, and (b) a mixed source (60% DC component + 40% ISO component).

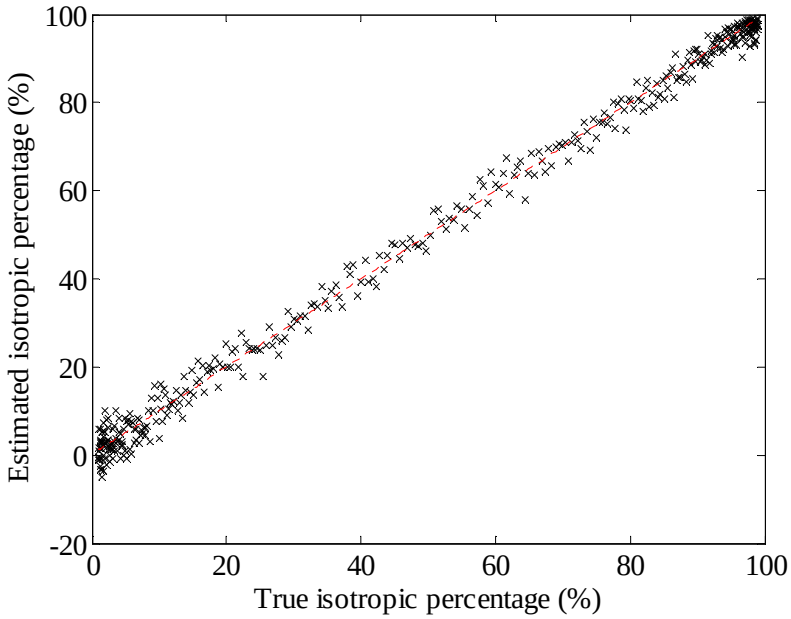

Figure 8. Comparison of the true and estimated isotropic percentage based on a Monte Carlo simulation with 10% additive Gaussian noise.

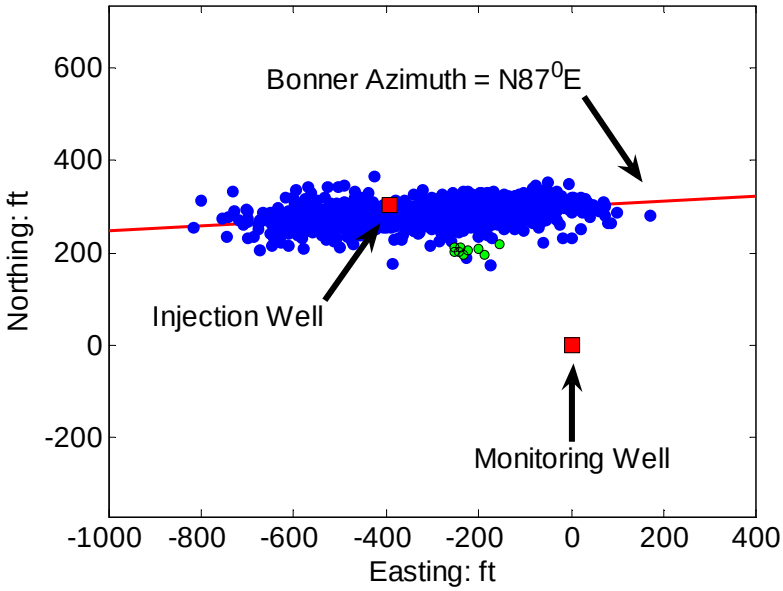

Figure 9. Horizontal plane view of microseismic event locations. Seven selected test events are shown in green.

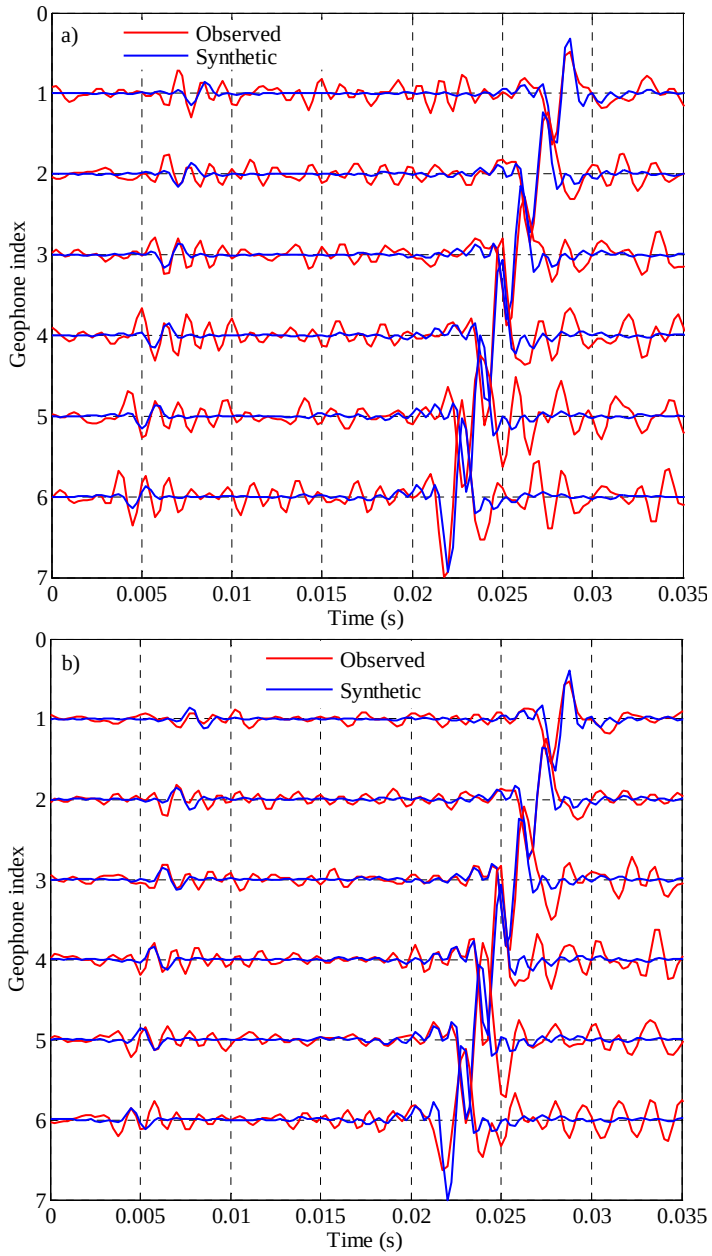

Figure 10. Comparison between the synthetics and observed data for test event 1: a) North component, b) East component.

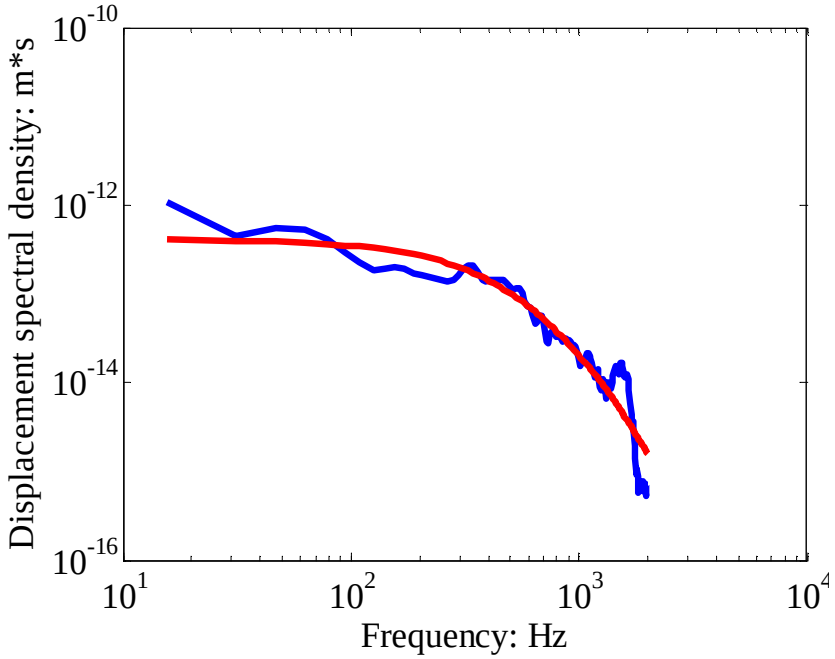

Figure 11. S-wave displacement spectrum of test event 1. The observed spectrum is shown in blue, and the model fitted result is plotted in red.

Table 1. Results of source parameter determinations.

Event	M_0	M_w	Strike	f_c	r_0	$\Delta\sigma$	ISO percentage
	10^4N·m		Degrees	Hz	m	Kpa	%
1	6.1	-2.87	102 12	481	1.2	15	-26
2	2.1	-3.17	80 207	561	1.0	8	29
3	8.1	-2.79	73 196	547	1.1	29	31
4	45	-2.29	139 39	564	1.0	178	30
5	5.3	-2.91	75 197	714	0.8	43	11
6	7.5	-2.81	95 211	736	0.8	66	-10
7	4.4	-2.96	82 203	744	0.8	40	-4

Note: strike is defined as East of North